

國立臺灣大學理學院大氣科學研究所



碩士論文

Department of Atmospheric Science

College of Science

National Taiwan University

Master Thesis

使用 Gamma 分布函數之總體水物法的水物終端速度參數化

Bulk Parameterization for Precipitation Particles' Terminal

Velocity for Gamma-type Particle Size Distribution

謝庭維

Ting-Wei Hsieh

指導教授：陳正平 教授

Advisor: Jen-Ping Chen, Ph.D.

中華民國 109 年 7 月

July, 2020

誌謝



敝生由衷感激陳正平老師的悉心指導、蔡子衿學長在 Fortran 程式語言上的幫忙，以及洪惠敏老師、林宜菽學姐與實驗室學長姐及同學提出的建議。

中文摘要



終端速度是雲物理學中的一個重要物理參數，對水物碰撞合併、重力沉降與凝結或蒸發的通風效應估算有密切關聯。本研究的目的旨在改進使用 gamma 粒徑分布函數的多矩量總體水物法模式中的水物終端速度參數式。針對雨滴部分，本研究基於 Böhm (1992) 的理論值進行參數化，並與 Gunn 與 Kinzer (1949) 比對以驗證參數式之可靠性；另有使用包含本研究參數式的數個參數法進行一維簡單重力沉降模式做數值動力測試。新的參數法相較於目前 WRF 模式中常見使用的終端速度參數式與前人研究成果之參數式更加準確。冰相水物的部分，本研究基於 Böhm (1989, 1992) 的理論值，除了冰相粒子大小與密度外，使用橢圓體近似得額外考慮冰晶形狀的影響。由於實驗研究資料仍不夠完備，冰晶參數法較難與目前實驗相互比對；但本研究將 Böhm (1989) 與目前較新亦較完整，由 Mitchell 與 Heymsfield (2005) 提出的架構進行比較。

關鍵字：終端速度、微物理參數化、總體水物法

ABSTRACT



Terminal velocity is a key parameter in cloud microphysical processes, including collision coalescence/accretion/aggregation, gravitational sedimentation, ventilation effect of hydrometeors' condensation/vaporization, etc. The goal of this study is to improve the terminal velocity parameterization for multi-moment hydrometeor microphysical schemes using gamma function as particle size distribution (PSD), which is the most common form of PSD in current bulk microphysical schemes. For raindrops, the semi-theoretical calculation of fall speed suggested by Böhm (1992) was used as the base of the parameterization. The results were compared with the experimental result of Gunn and Kinzer (1949) to check the liability of the parameterization. The new parameterization showed better accuracy compared with earlier formulas, including those used in the WRF model. For ice particles, the new parameterization can well approximate the fall speeds from the calculation framework of Böhm (1989, 1992) which considered not only the size and density dependence but also the shape of ice particles using spheroidal approximation. Verification of ice hydrometeors' fall speed is difficult because of the lack of comprehensive measurement data. Nevertheless, a comparison was made against the currently most comprehensive parameterization of Mitchell and Heymsfield (2005) that is based on a somewhat different analytical framework. A simple 1-D sedimentation dynamics test for raindrop terminal velocity is conducted to examine the behavior and usability of our parameterization formula.

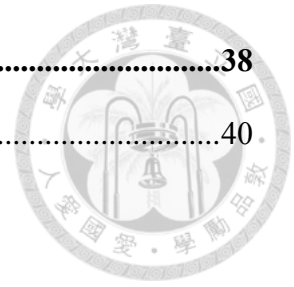
Keywords: terminal velocity, cloud microphysics, bulk parameterization

TABLE OF CONTENTS



口試委員會審定書	#
誌謝	i
中文摘要	ii
ABSTRACT	iii
TABLE OF CONTENTS	iv
LIST OF FIGURES	vi
LIST OF TABLES	viii
Chapter 1 Introduction	1
1.1 Raindrops	3
1.2 Ice particles	5
Chapter 2 Theoretical derivation of fall speeds	7
Chapter 3 Methodology	11
3.1 Database for parameterization	11
3.2 Fitting process	13
Chapter 4 Results	15
4.1 Parameterization of terminal velocity	15
4.2 Bulk fall speed	22
4.3 One-dimension simple dynamics test	24
Chapter 5 Discussion	28
5.1 Raindrops	28
5.2 Ice particles	33
5.3 Incorporation with other microphysical processes in models	36

Chapter 6 Conclusion38
REFERENCE40



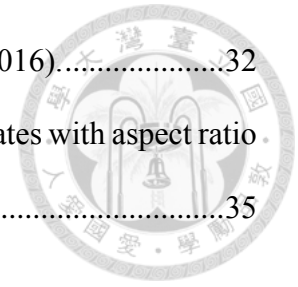
LIST OF FIGURES



Fig. 4.1:	Residuals of our user-defined formula and the built-in formulas provided with the TableCurve 3D software for raindrop, ice particles under 0.625mm in diameter and ice particles over 0.625mm in diameter.	17
Fig. 4.2:	Comparison between previously proposed parameterization formulas with this study.	20
Fig. 4.3:	Relative error of each formula comparing to the theoretical values from Böhm (1992).	21
Fig. 4.4:	Integral comparison between our parameterization formula for raindrops and the values derived from Böhm (1992).	22
Fig. 4.5:	Relative error of each formula comparing to the numerically integrated theoretical values from Böhm (1992).	23
Fig. 4.6:	Integral comparison between our parameterization formula for ice particles and the values derived from Böhm (1989).	24
Fig. 4.7:	Integral error of our formula for ice particles' comparing to numerical integral derived from Böhm (1989).	24
Fig. 4.8:	1-D simple dynamics test results.	27
Fig. 5.1:	The exponent of power-law relation between terminal velocity and diameter for raindrops.	29
Fig. 5.2:	Exponent in power-law relation between terminal velocity of raindrops and air density as a function of diameter under standard atmosphere profile.	30
Fig. 5.3:	Regression between terminal velocity and air density in Böhm (1992).	31
Fig. 5.4:	Comparison between Böhm (1992), our parameterization formula, Foote and	

duToit (1969), and experimental results from Yu et al. (2016).....32

Fig. 5.5: The difference between Böhm (1989) and MH05 for prolates with aspect ratio
of 100.....35



LIST OF TABLES



Table 3.1: Grid points used in deriving datum and fitting process.....	11
Table 4.1: Coefficients of raindrops' terminal velocity parameterization.	15
Table 4.2: Coefficients for the terminal velocity of ice particles under 0.625mm in diameter or $\mu/\lambda \leq 0.625$ mm.	15
Table 4.3: Details of coefficients in Table 4.2.	15
Table 4.4: Coefficients for the terminal velocity of ice particles over 0.625mm in diameter or $\mu/\lambda > 0.625$ mm.	16
Table 4.5: Details of coefficients in Table 4.4.	16
Table 4.6: Relative RMSE of terminal velocity prior to integration of different studies.	21

Chapter 1 Introduction



The fall speed of precipitation particle is an important but commonly overlooked physical parameter in current atmospheric models. Particles like raindrops and snow generally experience long falling distances in air with growth process taking time scales of minutes to hours, much greater than the time scale for such objects to reach terminal velocity – the fall speed that results in equilibrium between the pull of gravity and the drag applied to the objects by air:

$$F_{drag} = \frac{C_d}{2} A \rho_a v^2 = (m - V \rho_a) g = F_{grav} - F_{buoy} \quad (1.1)$$

where F is the applied force, with subscripts *drag*, *grav* and *buoy* representing the drag applied by the air, gravity and buoyancy, respectively C_d is drag coefficient; ρ_a is air density; m is mass of a particle; V is the volume of the particle; and g is the acceleration constant of gravity. Thus, the fall speed of precipitation particles is usually treated as constant downward motion at terminal velocity relative to the surrounding air. Accurate calculation of such property is crucial to the calculation of precipitation sedimentation along with other related physical processes such as coalescence and ventilation effect. Model simulations showed high sensitivity toward terminal velocity formulation, especially for ice particles (Tsai and Chen, 2020). Fall speed estimation may also have indirect impact on cloud lifetime and thickness, which may have impact on the radiative forcing in models.

Since parameters describing the properties of particles are represented in moments for bulk microphysical parameterization schemes, the fall speed formulas have to be integrated with the particle size distribution (PSD) functions in order to acquire the time

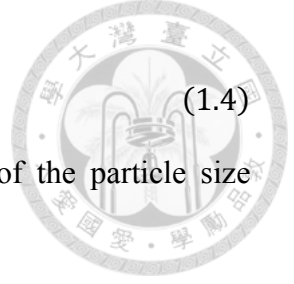
derivatives of those variables. For single and double moment implementations adopting bulk parameterization microphysical schemes, particle size distribution suggested by Marshall and Palmer (1948) is widely used. However, observation results suggest that the number concentration of particles according to their sizes peaks at certain non-zero diameter, which Marshall-Palmer distribution does not present (Tokay and Short, 1996). In order to achieve more accurate microphysical process simulations in models, triple moment bulk parameterization schemes are emerging as the new norm, and the use of gamma distribution function to describe approximated PSD, suggested by Ulbrich (1983) is commonly adopted in both triple moment models like the NTU scheme (Tsai and Chen 2020) as the following:

$$N(D) = N_0 D^\mu e^{-\Lambda D} \quad (1.2)$$

where N is the number concentration, D is particles' diameter, and N_0, μ, Λ are parameters describing the shape of the PSD function. The integration moment of the gamma distribution function can be derived with the following analytical solution:

$$M_{(k)} \equiv \int_0^{\infty} N(D) D^k dD = \int_0^{\infty} N_0 D^{\mu+k} e^{-\Lambda D} dD = \frac{N_0 \Gamma(\mu + k + 1)}{\Lambda^{\mu+k+1}} \quad (1.3)$$

where M_k is the k^{th} moment, and $\Gamma(x)$ is the gamma function. In fact, the Marshall-Palmer distribution may be seen as a simplified gamma distribution function with $\mu = 0$. For model computation to be practically efficient, formulas of particles' terminal velocity must emit analytical solution when integrated with corresponding PSD functions. Unfortunately, complexity of existing theoretical computation for hydrometer terminal velocity renders it implausible to derive corresponding analytical integrals with bulk parameterization, thus further simplification for terminal velocity prediction is required. Approximations in form of power-laws are generally used in bulk parameterizations implemented in models like WRF.



$$v = aD^b \quad (1.4)$$

Such formulation may be easily integrated analytically for most of the particle size distribution functions as the following:

$$\bar{v}_{\langle k \rangle} = \frac{\int_0^\infty aD^b N_0 D^{\mu+k} e^{-\Lambda D} dD}{\int_0^\infty N_0 D^{\mu+k} e^{-\Lambda D} dD} = \frac{a \Gamma(\mu + k + b + 1)}{\Gamma(\mu + k + 1) \Lambda^b} \quad (1.5)$$

where $\bar{v}_{\langle k \rangle}$ is the bulk fall speed of the k^{th} moment. Nonetheless, experiment result from Gunn and Kinzer (1949) and theoretical calculation proposed by Böhm (1989, 1992) already suggested that such approximation may not be adequately accurate. For small particles with Reynolds number ranging in the laminar flow regime, the terminal velocity is approximately proportional to D^2 . With the particle growing larger and resulting in higher Reynolds number, the vortex wakes starts to form, and the flow regime transits to Oseen flow, where the terminal velocity is around the scale D^1 . For even larger particles with high Reynolds number, the flow around particles become turbulent, hence the terminal velocity approaches to where it is roughly proportional to $D^{1/2}$.

1.1 Raindrops

For raindrops, the particles may deform due to the extra pressure pushing on the liquid facing towards the moving direction. The effect is greater for large particles, thus for small particles as cloud droplets and drizzle, the particles may still be considered as spherical. For raindrops larger than 1 mm in diameter, such effect starts to flatten the droplets and increase the cross-section area facing downwards, rendering the actual terminal velocity to be lower than that of a sphere with the same mass and volume. Experimental result from Gunn and Kinzer (1949) suggests such effect flattens the curve of terminal velocity-size according to particles' dimensions for large particles and the

deviation from fixed power law cannot be omitted for droplets larger than 1 mm in diameter.



Several empirical or parameterization formulas are suggested in previous studies. Best (1950) proposed one of the earliest empirical formula using experimental data including those from Gunn and Kinzer (1949) expressed as the following:

$$v = 9.32e^{0.0405z}(1 - e^{(D/1.77)^{1.147}}), \quad (1.6)$$

where z is altitude in km and D is diameter in mm, with fall speed v in m/s. The formula contains the idea of expressing the phenomenon that the terminal velocity curve flattens in the large drop size regime by using exponential asymptote. Nevertheless, the formula involves a power-law term of diameter in the exponent, thus cannot be analytically integrated with gamma PSD function in traditional bulk parameterization. Atlas et al. (1973) proposed another empirical formula as a part of Doppler radar data derivation:

$$v = 9.65 - 10.3e^{-0.6D}, \quad (1.7)$$

where D is diameter in mm and fall speed is in m/s. This formula also involves exponential asymptote to describe the flattened curve, and is in the form that allows analytical integration with gamma PSD function available. However, the formula is only fitted for a single temperature-pressure condition and lacks the expression for varying air property. Lhermitte (1990) published a formula by using a similar tactic to fit the experimental data from Gunn and Kinzer (1949):

$$v = 9.23(1 - e^{-0.68D^2 - 0.488D}) \left(\frac{\rho_{a,0}}{\rho_a} \right)^{0.5}, \quad (1.8)$$

where D is diameter in mm, with fall speed in m/s. This formula does not give analytical integral with arbitrary gamma PSD function either, as it involves D^2 in its exponent. Formulas based on power-law function as given in equation (1.4) have been proposed

by Atlas and Ulbrich (1977), Rogers (1989), Rogers and Yau (1989), as well as that applied in WDM6 microphysical scheme. The exponent coefficient that used in these formulas ranges from 1 to 0.5; many of them also considered the air density term similar to that given in equation (1.8), with the exponent coefficient ranging from -0.4 to -0.5. The Thompson microphysical scheme adopted another approach by directly multiplying an exponential term to a power-law relation of diameter:

$$v = 4.854De^{-0.195D} \left(\frac{\rho_{a,0}}{\rho_a} \right)^{0.5}, \quad (1.9)$$

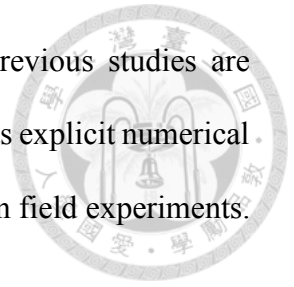
where D is diameter in mm, with output fall speed in m/s. The formula fits the data from Gunn and Kinzer (1949) quite well and covers the range of diameter between 0 and 6 mm with decent accuracy.

1.2 Ice particles

For ice particles, the particles' shape plays an important role in determining the terminal velocity. Ice particles' shape effect is commonly expressed with an independent variable such as the aspect ratio (e.g., Böhm, 1989) or using the area/mass-dimension relation (e.g. Mitchell and Heymsfield, 2005; Khvorostyanov and Curry, 2005) in different frameworks. The fall speed of non-spherical particles has been derived by Böhm (1992). Although ice particles do not deform like raindrops do, the number of variables that control fall speed is greater due to the large variation in shape and density. Ice crystals may grow in specific patterns, introducing gaps and air chambers in them; snow aggregates and graupeln also enclose air packets during growth process. Thus, the apparent density can be lower than the bulk density of ice. Model results suggest that effective density could be as low as 50 kg/m^3 . Moreover, the ice particles' surfaces are likely to have irregularity and should also be taken into account and as discussed by Böhm

(1989). Parameterization formulas for ice particles proposed by previous studies are mostly empirical and are categorized by the type of ice hydrometeor, as explicit numerical values describing the properties such as shapes are hardly available in field experiments.

(Pruppacher and Klett, 2010)



Chapter 2 Theoretical derivation of fall speeds



From equation (1.1), the drag coefficient is however a conventionally adopted treatment to simplify the expression of Reynolds number and is not an independent variable to particles' diameter. Thus the terminal velocity may not be directly retrieved by simply rearranging equation (1.1) and taking square root on both side. Proper drag coefficient retrieval requires solving Navier-Stokes and continuity equations describing the flow pattern around the object under constant background flow.

For sufficiently small Reynolds number under steady state, analytical solution for smooth spherical particles is well known as Stokes flow. Scale analysis shows inertia term is relevantly insignificant comparing to viscous drag under this regime and can be neglected:

$$\frac{|(\vec{u} \cdot \nabla)\vec{u}|}{|\nu \nabla^2 \vec{u}|} \approx \frac{U^2/D}{\nu U/D^2} = \frac{UD}{\nu} \equiv N_{Re} \ll 1 \quad (2.1)$$

where \vec{u} is the fluid velocity, ν is dynamic viscosity, U is the background flow speed, and D is the diameter of the object. The resulting linearized Navier-Stokes equation then can be solved, which gives the drag force applied on a particle as:

$$F_{drag} = 3\pi D\eta U. \quad (2.2)$$

The expression may also be written in form of drag coefficient:

$$C_d \equiv \frac{F_{drag}}{(\rho_a U^2/2)A} = \frac{3\pi D\eta U}{\left(\frac{\rho_a U^2}{2}\right)\left(\frac{\pi D^2}{4}\right)} = \frac{24}{N_{Re}} \quad (2.3)$$

By substituting equation (2.2) into equation (1.1), and replacing, we then have:

$$3\pi D\eta v = (m - V\rho_a)g. \quad (2.4)$$

With the assumption that the particle is a homogeneous sphere with density ρ_a , we may retrieve its terminal velocity as the following:

$$v = \frac{D^2 g (\rho - \rho_a)}{18\eta}. \quad (2.5)$$

The solution may be extended to the regime under higher Reynolds number known as the Oseen flow, where the inertia term is linearized as $(\vec{U} \cdot \nabla)\vec{u}$ instead of being completely discarded. The resulting drag force formula is:

$$F_{drag} = 3\pi D\eta U \left(1 + \frac{3}{16} N_{Re}\right), \quad (2.6)$$

or in drag coefficient expression:

$$C_d = \frac{24}{N_{Re}} + \frac{9}{2}$$

which leads to a quadratic equation of terminal velocity as the following:

$$3\pi D\eta v + \frac{9}{16} \pi \rho_a D^2 v^2 = \frac{\pi D^3}{6} g (\rho - \rho_a). \quad (2.7)$$

For small particles, the formula approaches the behavior of Stokes terminal velocity; then it is followed by a transition regime where the terminal velocity is proportional to about D and slowly approaches the scaling of $D^{1/2}$. Also the viscosity is less relevant for larger particles where inertia term has more effect. (Pruppacher and Klett, 2010, chap. 10)

However, for regimes with even larger Reynolds number, the steady state assumption used to derive those solutions does not hold. Böhm (1989) derived an analytical framework utilizing the Best (or Davies) number, X :

$$X \equiv \frac{2mg\rho_a D_*^2}{A\eta^2} = C_d N_{Re}^2 \quad (2.8)$$

where η is the kinematic viscosity of air, $D_* \equiv 2\sqrt{A_*/\pi}$ where A_* is defined as the minimal ellipse covering the maximum cross section area of the particle, and N_{Re} is the Reynold's number. The drag coefficient C_d may be formulated using boundary layer theory for N_{Re} greater than δ_0^2 :

$$C_d = C_0 \left(1 + \frac{\delta_0}{\sqrt{N_{Re}}} \right)^2, \quad (2.9)$$

in which C_0 and δ_0 are parameters related to the surface roughness and shape of particles. Combining eqs. (2.1) and (2.2) gives a quadratic equation of $N_{Re}(X)$, which gives two roots and only the positive one is applicable:

$$N_{Re,0}(X) = \frac{6k}{C_0} \beta^2, \quad (2.10)$$

where β is defined as:

$$\beta \equiv \sqrt{1 + \frac{C_0}{6k} \sqrt{\frac{X}{C_0}}} - 1, \quad (2.11)$$

with k being another shape-related parameter. For the flow regime where $N_{Re} \ll 1$ and creeping motion is the dominant dynamics, the drag coefficient should approach to the scaling of N_{Re}^{-1} ; however, boundary layer theory does not give such limit. Thus, a correction parameter derived from perturbation theory may be applied as the following:

$$N_{Re} = N_{Re,0} \left[1 + \frac{2\beta e^{-\beta\gamma}}{(2 + \beta)(1 + \beta)} \right] \quad (2.12)$$

where γ is a constant. With Reynold's number known, the terminal velocity may then be calculated as:

$$v = \frac{N_{Re}\eta}{\rho_a D_*} \quad (2.13)$$

For Reynold's number greater than 10^3 , a turbulence transition induced correction

should be applied for calculating the Best or Davies number X . The empirical formula determines the drag coefficient for turbulent flow regime:

$$\frac{C_d'}{C_d} = \frac{X'}{X} = \frac{1 + 1.6 \left(\frac{X}{X_0}\right)^2}{1 + \left(\frac{X}{X_0}\right)^2}, \quad (2.14)$$

in which X_0 is a constant depending on the roughness of particles, and X' should be used instead of X to determine the Reynold's number.

For raindrops, spherical parameters with $k \equiv 1$ is used along with linear shape-correction as it already gives adequately accurate results comparing to the experiment results by Gunn and Kinzer (1949). The correction parameter is given as:

$$v_c = v \cdot [\max(1, 0.90025 + \alpha D)]^{-1} \quad (2.15)$$

where $\alpha = 0.053635 \text{ mm}^{-1}$. Also, since deviation of shape from being spherical introduces ambiguity for the definition of particles' diameter, D is then defined as equivalent diameter, interpreted as the diameter of a sphere with the same volume of a particle:

$$D \equiv \sqrt[3]{\frac{6V}{\pi}} \quad (2.16)$$

Chapter 3 Methodology



3.1 Database for parameterization

The parameterization will use analytical values of fall speed for fitting. The analytical values used in the parameterization are mainly derived from Böhm (1989, 1992) (Table 3.1).

Table 3.1: Grid points used in deriving datum and fitting process.

	Range	Intervals
Diameter ⁺	50 μm to 9 mm	2 μm for diameter less than 100 μm 50 μm , else.
Diameter ^{**}	5 μm to 20 mm	5 μm for diameter less than 1.25 mm 100 μm , else.
Pressure [*]	200 hPa – 1100 hPa	75 hPa
Temperature [*]	Standard atmosphere \pm 10 K	2.5 K
Particle density ^{**}	50 kg/m^3 – 900 kg/m^3	50 kg/m^3

⁺ For raindrops only.

^{*} For both raindrops and ice particles.

^{**} For ice particles only.

For raindrops, since the particle deformation corrections given in literatures provided only a dependence on particles' diameter, the terminal velocity hence is treated as a function of diameter and the property of surround air. The parameters for equations (2.9) to (2.12) are set as the following as suggested in Böhm (1992): $C_0 = 0.292$, $X_0 = 6.7 \times 10^6$, and $\gamma = 3.6$.

For ice particles, their shapes are represented by spheroids, and the shape parameter of them may be represented by the aspect ratio, denoted as ϕ :

$$\phi \equiv \frac{c}{a}. \tag{3.1}$$

with a defined as the equatorial radius, and c as the poleward radius or the distance

between the pole and the center of a spheroid. As the volume of a spheroid can be expressed as $V = \frac{4\pi}{3} a^2 c$, we then have the relationship between diameter D , a and c :

$$D = 2\sqrt[3]{a^2 c} \quad (3.2)$$

$$a = \sqrt[3]{\phi^{-1}} D/2 \quad (3.3)$$

$$c = \sqrt[3]{\phi^2} D/2 \quad (3.4)$$

Such assumption leads to a correction factor for the Best number, X , when dealing with the surface irregularity. The factor is not considered in the scope of this study, thus the cross-section area is calculated as the downward projected ellipse of the spheroid describing the particle:

$$A = \begin{cases} \pi a^2, & \text{for oblates;} \\ \pi a c, & \text{for prolates.} \end{cases} \quad (3.5)$$

Thus, the Best number can be rearranged as the following:

$$X \equiv \frac{4D^3 \rho_i g \rho_a}{3\eta^2} \quad (3.6)$$

where ρ_i is the apparent density of ice particles, defined as the mass divided by the volume of describing spheroid.

Another criterion has to be met in the NTU microphysics scheme for ice crystal growth habit as proposed by Chen and Lamb (1994) is the aspect ratio of pristine ice crystals to follow a power-law relationship with diameter (cf. Chen and Tsai 2016):

$$\phi = \left(\frac{D}{D_0}\right)^{\xi(T)} \quad (3.7)$$

where D_0 is a constant of 6 μm , and ξ is a function solely depending on air temperature. Such a restriction limited the formulation of ϕ to also follow a power-law form in the terminal velocity parameterization for gamma-type PSD. Also, ϕ is an independent term and can be separated from other parameters during the evaluation of C_d . By contrast, the

shape parameter ϕ in Böhm (1992) is contained in a logarithmic term, which makes it incompatible with for the gamma-type PSD. Hence, the simpler form proposed in Böhm (1989) instead of the full-fledged formulation in Böhm (1992) is used in this study. In this way, the aspect ratio is introduced only in the last step of terminal velocity calculation (equation 2.6), which gives:

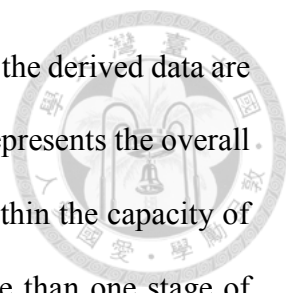
$$v = \begin{cases} \frac{N_{Re}\eta}{\rho_a D} \cdot \phi^{1/3}, & \text{for oblates;} \\ \frac{N_{Re}\eta}{\rho_a D} \cdot \phi^{-1/6}, & \text{for prolates.} \end{cases} \quad (3.8)$$

The resulting formulation of ϕ then is already parameterized and does not require additional fitting. The constant C_0 is chosen to be 0.6 as suggested by Böhm (1989).

3.2 Fitting process

The kernel transformation (SNAP-KT) approach (Chen et al., 2013) is used to create the parameterization formula. The method involves transforming or approximating the complicated integration kernel into mathematically manageable forms that then can be integrated analytically with the gamma-type PSD functions. In other words, this approach focuses on approximating formulas that cannot give analytical integrals with corresponding PSD function by ones that emits analytical integrals. The SNAP-KT approach was adopted as accurate terminal velocity parameterization may also be important while being with other relevant microphysical processes. This method may allow other parameters, under proper parameterization, being directly applied to the terminal velocity formula, which then also can be analytically integrated with PSD functions.

The software in use is TableCurve 3D, as it can efficiently process non-linear two-



variable functions with reasonable statistical accuracy. For raindrops, the derived data are fitted against equivalent particle diameter and air density, the latter represents the overall air properties. Such a two-variable (size and air density) fitting is within the capacity of the software, whereas more dependent variables would require more than one stage of curve fitting. For example, treatment for ice particles requires additional fitting against the equivalent particle density. For such an situation, the particles' diameter and air density are fed into the fitting process under a given apparent particle density first with a fixed form of formulas; then, each resulted fitting coefficient is fitted against ice apparent density.

The resulting raindrop formulas are compared to the theoretical values derived from Böhm (1992), and the ice particle formulas are compared to values derived from Böhm (1989). Since the ground truth of hydrometeors' terminal velocity has not yet come to a consensus in previous studies, the errors are hence defined as the deviations of the mentioned comparisons. The “bulk fall speeds” in equation (1.5) pertaining to each moment are the formulas eventually used in bulk parameterizations, so the final evaluation should be performed in terms of bulk fall speeds. For such comparisons, PSD parameters derived from Willis et al. (1999) with rain water mixing ratio in the range of 0 to 5 g/m³ in logarithmic intervals are used for raindrops; and for ice particles the range of $0 \leq \mu \leq 5$ and $0 \leq \lambda \leq 60 \text{ mm}^{-1}$ in linear intervals are chosen to cover the observational regression results from McFarquhar et al. (2014). For the “ground-truth” formulas that do not yield a analytical solution to the integral, numerical integration is used instead.

Chapter 4 Results



4.1 Parameterization of terminal velocity

Equations approximating terminal velocity suitable for usage in bulk parameterization using gamma PSD are fitted for both raindrops and ice particles in the following form:

$$v \cong f(\phi) \sum_i a_i D^{b_i} e^{-\lambda_i D} \quad (4.1)$$

$$f(\phi) = \begin{cases} \phi^{1/3}, & \text{for oblates;} \\ \phi^{-1/6}, & \text{for prolates.} \end{cases} \quad (4.2)$$

where A_i , b_i and λ_i are coefficients that may be functions of air density and, for ice particles, the particles' apparent density (Table 4.1 to Table 4.5). Note that $f(\phi)$ is only needed for ice particles, although one can also apply $\phi=1$ for spherical particles.

Table 4.1: Coefficients of raindrops' terminal velocity parameterization. ($q = \exp(0.115231 \cdot \rho_a)$, ρ_a in kg/m^3 , c_i in mm^{-1} , a_i is in $\text{m}^{-3}\text{mm}^{-(1+b_i)}$.)

i	a_i	b_i	c_i
1	$0.044612 \cdot q$	$2.2955 - 0.038465 \cdot \rho_a$	0
2	$-0.263166 \cdot q$	$2.2955 - 0.038465 \cdot \rho_a$	0.184325
3	$4.7178 \cdot q \cdot \rho_a^{-0.47335}$	$1.1451 - 0.038465 \cdot \rho_a$	0.184325

Table 4.2: Coefficients for the terminal velocity of ice particles under 0.625 mm in diameter for single particle or $\mu/\Lambda \leq 0.625$ mm for bulk parameterization. (ρ_a in kg/m^3 , c_i in mm^{-1} , a_i is in $\text{m}^{-3}\text{mm}^{-(1+b_i)}$; details of the coefficients are given in Table 4.3.)

i	a_i	b_i	c_i
1	$E_s \cdot \rho_a^{A_s}$	$B_s + C_s \cdot \rho_a$	0
2	$F_s \cdot \rho_a^{A_s}$	$B_s + C_s \cdot \rho_a$	G_s

Table 4.3: Details of the coefficients in Table 4.2, where ρ_i is the apparent density of ice particles in kg/m^3 .

A_s	$-0.263503 + 0.00174079 \ln^2(\rho_i) - 0.0378769 \ln(\rho_i)$
-------	--

B_s	$\left(0.575231 + 0.0909307 \ln(\rho_i) + 0.515579 \rho_i^{-1/2}\right)^{-1}$
C_s	$-0.345387 + 0.177362 \exp(-0.000427794 \rho_i) + 0.00419647 \rho_i^{1/2}$
E_s	$-0.156593 - 0.0189334 \ln^2(\rho_i) + 0.1377817 \rho_i^{1/2}$
F_s	$-\exp(-3.35641 - 0.0156199 \ln^2(\rho_i) + 0.765337 \ln(\rho_i))$
G_s	$\left(-0.0309715 + 1.55054 / \ln(\rho_i) - 0.518349 \ln(\rho_i) / \rho_i\right)^{-1}$

Table 4.4: Coefficients for the terminal velocity of ice particles larger than 0.625 mm in diameter for single particle or $\mu/\Lambda > 0.625$ mm for bulk parameterization. (ρ_a in kg/m^3 , c_i in mm^{-1} , a_i is in $\text{m}^{-3} \text{mm}^{-(1+b_i)}$; details of the coefficient are given in Table 4.5.)

i	a_i	b_i	c_i
1	$B_L \cdot \rho_a^{A_L}$	C_L	0
2	$E_L \cdot \rho_a^{A_L} \cdot \exp(H_L \cdot \rho_a)$	F_L	G_L

Table 4.5: Details of the coefficients in Table 4.4, where ρ_i is the apparent density of ice particles in kg/m^3 .

A_L	$-0.475897 - 0.00231270 \ln(\rho_i) + 1.12293 \rho_i^{-3/2}$
B_L	$\exp(-2.56289 - 0.00513504 \ln^2(\rho_i) + 0.608459 \ln(\rho_i))$
C_L	$\exp\left(-0.756064 + 0.935922 / \ln(\rho_i) - 1.70952 \rho_i^{-1}\right)$
E_L	$0.00639847 + 0.00906454 \ln(\rho_i) \rho_i^{1/2} - 0.108232 \rho_i^{1/2}$
F_L	$0.515453 - 0.0725042 \ln(\rho_i) - 1.86810 \times 10^{19} \exp(-\rho_i)$
G_L	$\left(2.65236 + 0.00158269 \ln(\rho_i) \rho_i^{1/2} + 259.935 \rho_i^{-1/2}\right)^{-1}$
H_L	$-0.346044 - 7.17829 \times 10^{-11} \rho_i^{5/2} - 1.24394 \times 10^{20} \exp(-\rho_i)$

While TableCurve 3D comes with numerous built-in equations that can be used automatically to evaluate the fitting, it also allows user-provided formulas. This study found a customized (user-defined) formula that gives much better results with R^2 greater

than 0.998 and 0.999, comparing to built-in formulas that have R^2 capped at 0.92 and 0.998 (not including the error introduced by apparent density) for raindrops and ice particles, respectively, under the analytical integration constrain (Fig. 4.1).

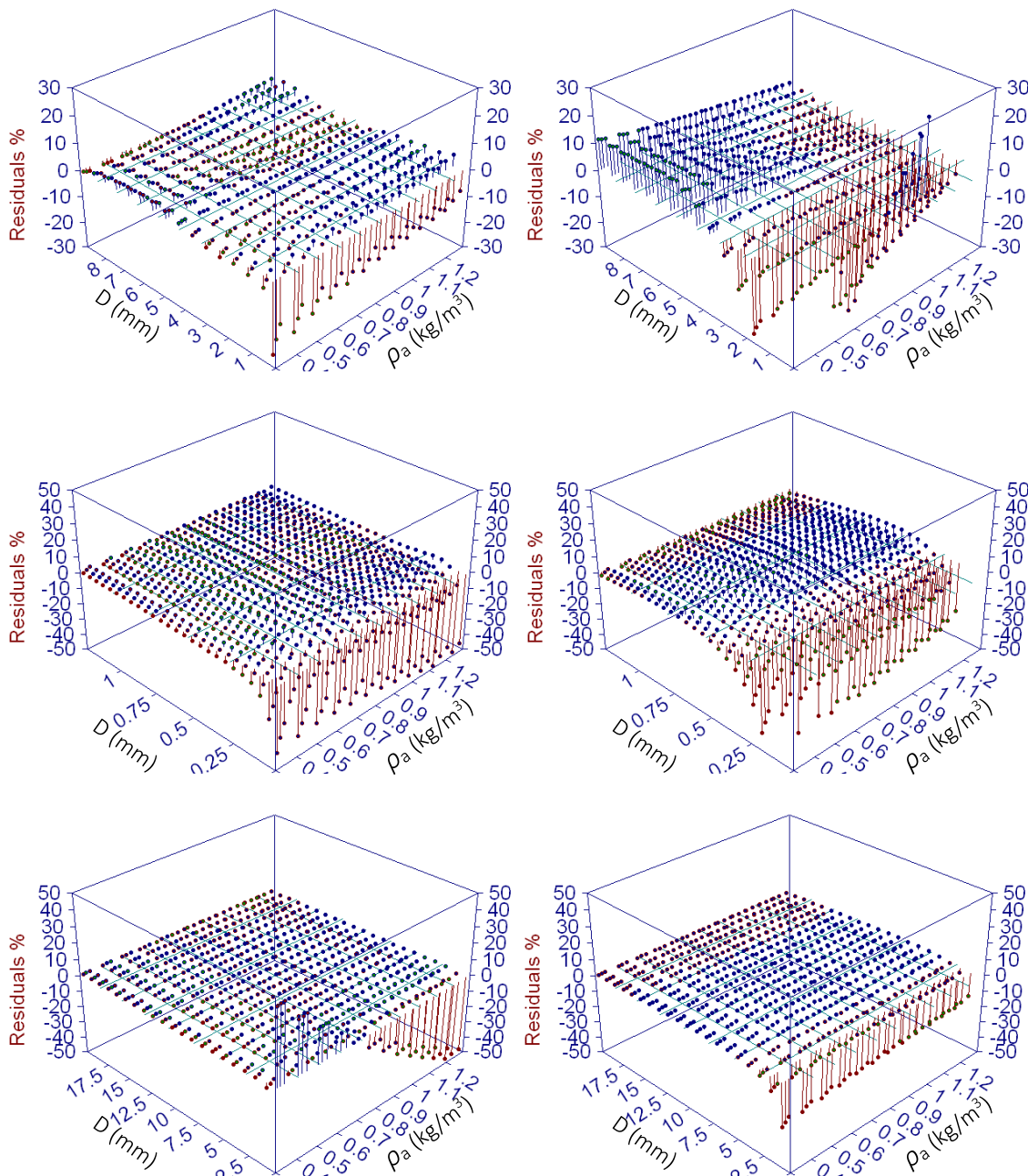
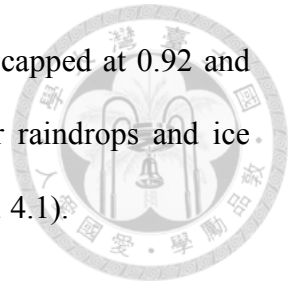
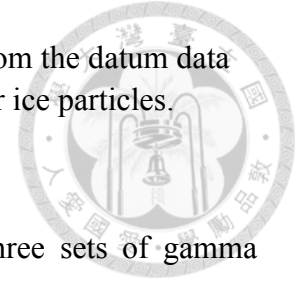


Fig. 4.1: Residuals of our user-defined formula (left column) and the built-in formulas provided with the TableCurve 3D software (right column) for raindrops (top row), ice particles under 0.625mm in diameter (middle row) and ice particles over 0.625mm in diameter (bottom row). The colored circles are the values derived from fitted formulas,

with vertical lines connecting the circles indicating the deviation from the datum data derived from Böhm (1992) for raindrops and Böhm (1989) for ice particles.

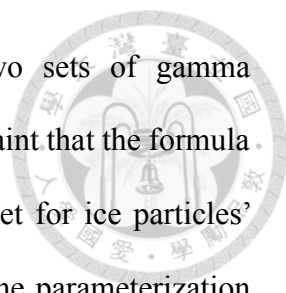


For raindrops, the formula is continuous and consisted of three sets of gamma distribution function ($i = 1, 2, 3$), suitable for droplets larger than 100 μm in diameter. The formula does not converge strictly to zero for a zero size, indicating that it is not suitable for extrapolating to cloud drop sizes. However, cloud droplets' terminal velocity may be well described by the Stokes flow with a robust dependence on D^2 and thus does not require parameterization.

Fig. 4.2 shows a comparison between our parameterization formula, the theoretical data from Böhm (1992), and several previous studies for raindrops. Formulas using power-law relation (Atlas and Ulbrich, 1977; Rogers, 1989; Rogers and Yau, 1989; WDM6 microphysical scheme) behaves significantly poorer for larger droplets than those using exponential asymptote (Best, 1950; Atlas et al., 1973; Lhermitte, 1990), as well as that of the Thompson microphysical scheme which cannot express the curve-flattening phenomenon in the large-size region. When using such formulas, an upper limit must be applied to either the fall speed (such as the Morrison scheme) or the raindrop size (such as the WDM6 scheme) to avoid exaggerated sedimentation. The relative root mean square error (RMSE), defined as follows, of formulas prior to integration is listed in Table 4.1:

$$\text{RMSE} \equiv \sqrt{\frac{\sum_{i=1}^n \left(\frac{v_{*,i} - v_i}{v_i} \right)^2}{n}} \quad (4.3)$$

where n is the number of data points, i is the dummy index, v_i is the theoretical value and $v_{*,i}$ is the parameterization value.



For ice particles, the parameterization formula contains two sets of gamma distribution function ($i = 1, 2$). However, unlike raindrops, the constraint that the formula must approach zero when the diameter reduces to zero must be met for ice particles' parameterization in the NTU as its PSD has no lower size limit. The parameterization formula must also cover very large ice particles such as hailstones, thus the applicable largest diameter is set at 20 mm instead of 9 mm for raindrops. To accommodate such a large size range, the parameterization is divided into two size sections with the modal size (in equivalent diameter) cut at 625 μm .

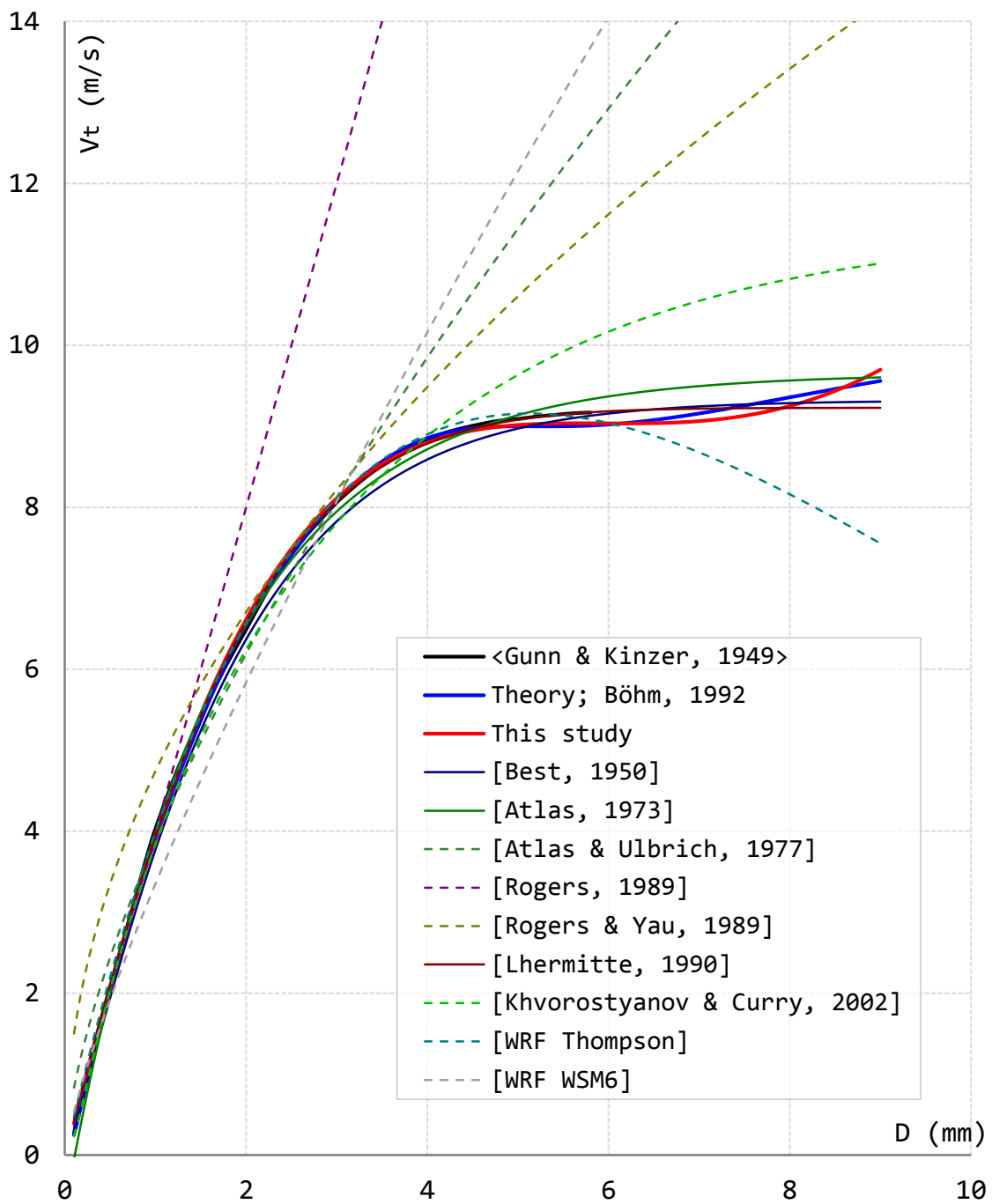


Fig. 4.2: Comparison between previously proposed parameterization formulas with this study. (Under $P = 1010\text{hPa}$ and $T = 20^\circ\text{C}$.)

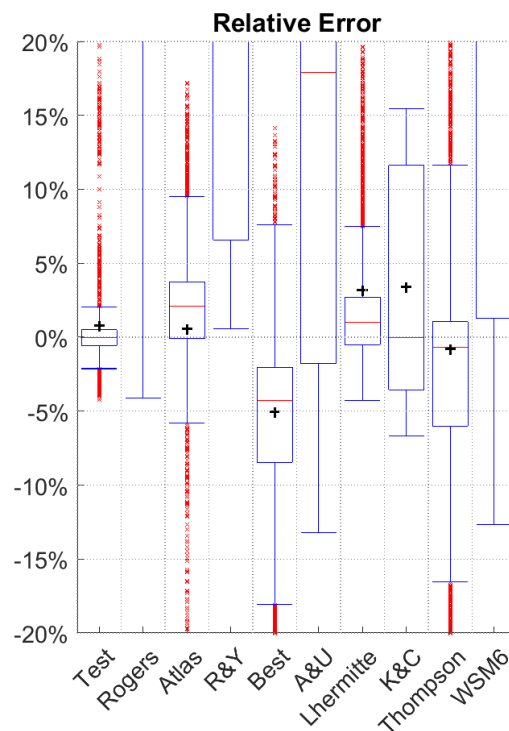
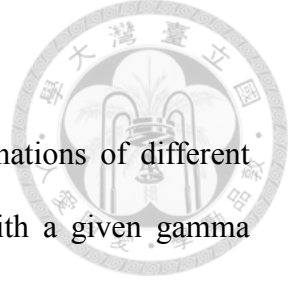


Fig. 4.3: Relative error of each formula comparing to the theoretical values from Böhm (1992). Black plus signs are mean relative errors; red horizontal lines are medians, blue boxes represent 25th (Q₁) and 75th (Q₃) percentiles, top blue lines are either the maximum values or Q₃ + 1.5 (Q₃ - Q₁), bottom blue lines are either the minimum values or Q₁ - 1.5 (Q₃ - Q₁), values beyond the ranges covered by blue lines are represented in red dots. The PSD parameters used in integrals are derived from Willis et al. (1999). From left to right in each sub-figure are the error margin respectively for our new formula (dubbed as “Test”), Rogers (1989), Atlas et al. (1973), Rogers and Yau (1989), Best (1950), Atlas and Ulbrich (1977), Lhermitte (1990), Khvorostyanov and Curry (2002), Thompson microphysical scheme, and WDM6 microphysical scheme.

Table 4.6: Relative RMSE of terminal velocity prior to integration of different studies.

Study	Relative RMSE
This study	6.4%
Rogers (1989)	> 100%
Atlas et al. (1973)	13.6%
Rogers and Yau (1989)	73.3%
Best (1950)	9.1%
Atlas and Ulbrich (1977)	44.5%
Lhermitte (1990)	12.5%
Khvorostyanov and Curry (2002)	8.2%
WRF Thompson	15.3%
WRF WDM6	55.8%



4.2 Bulk fall speed

The formulas derived above are in the form of linear combinations of different gamma distribution function, thus the result may be integrated with a given gamma particle size distribution:

$$\bar{v}_{\langle k \rangle} \equiv \frac{\int_0^\infty N_0 D^{\mu+k} e^{-\Lambda D} v(D) dD}{\int_0^\infty N_0 D^{\mu+k} e^{-\Lambda D} dD} \cong f(\phi) \sum_i \frac{a_i \Lambda^{\mu+k+1} \Gamma(\mu + b_i + k + 1)}{(\Lambda + c_i)^{\mu+b_i+k+1} \Gamma(\mu + k + 1)}. \quad (4.4)$$

The performance of the parameterizations can also be examined in terms of the bulk fall speeds as indicated in equation (4.4). Fig. 4.5 compares the bulk fall speeds for the zeroth, second and third moments according to various parameterizations. One can see that the formula obtained in this study shows significant improvement in accuracy against those from previous studies.

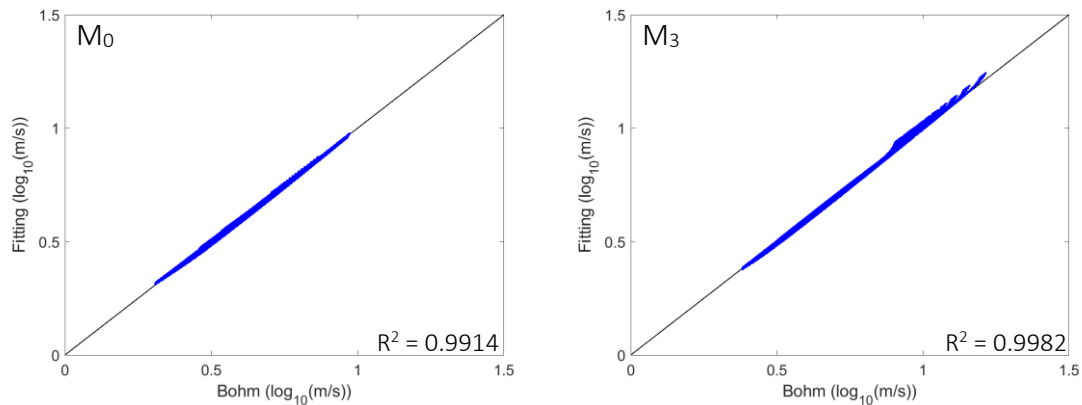


Fig. 4.4: Integral comparison between our parameterization formula for raindrops and the values derived from Böhm (1992). The gamma PSD parameters are derived from Willis et al. (1999).

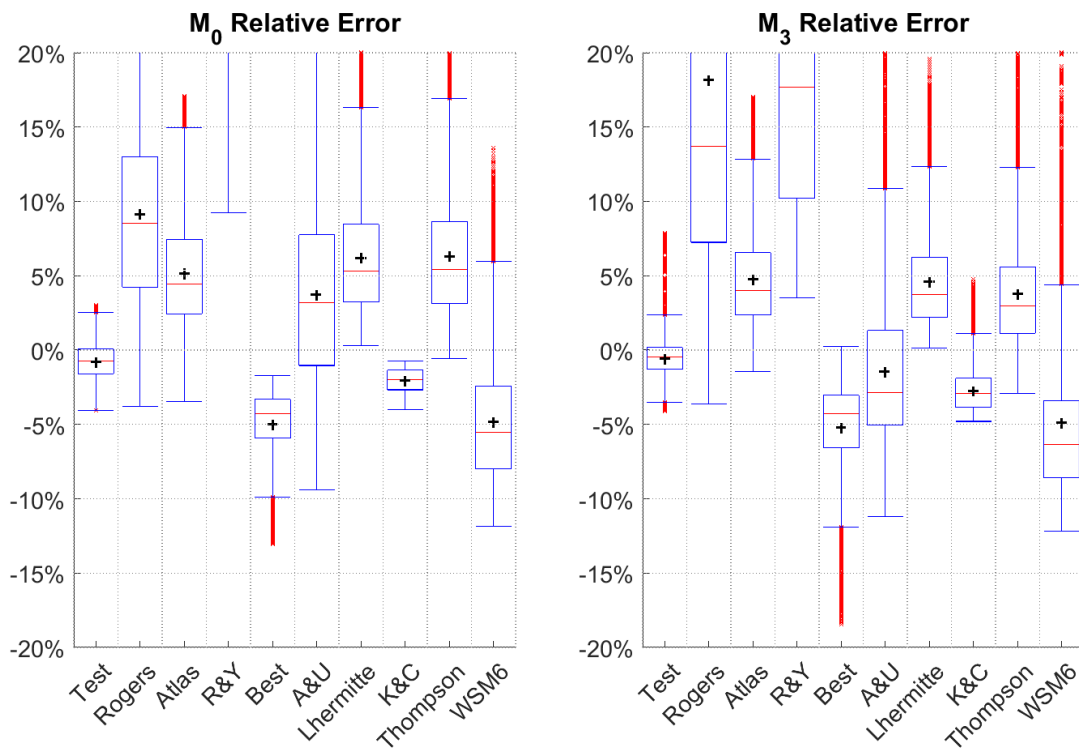


Fig. 4.5: Relative error of each formula comparing to the numerically integrated theoretical values from Böhm (1992). The left figure is the 0th moment kernel, and the right is 3rd moment kernel (2nd moment not shown). The gamma PSD parameters are derived from Willis et al. (1999), with median diameter mostly falls around 1 mm. Black plus signs are mean relative errors; red horizontal lines are medians, blue boxes represent 25th (Q₁) and 75th (Q₃) percentiles, top blue lines are either the maximum values or Q₃ + 1.5 (Q₃ - Q₁), bottom blue lines are either the minimum values or Q₁ - 1.5 (Q₃ - Q₁), values beyond the ranges covered by blue lines are represented in red dots. The PSD parameters used in integrals are derived from Willis et al. (1999). From left to right in each sub-figure are the error margin respectively for our new formula (dubbed as “Test”), Rogers (1989), Atlas et al. (1973), Rogers and Yau (1989), Best (1950), Atlas and Ulbrich (1977), Lhermitte (1990), Khvorostyanov and Curry (2002), Thompson microphysical scheme, and WDM6 microphysical scheme. The data derived from Khvorostyanov and Curry (2002) in this study does not involve optimal size selection and is integrated numerically (see chap. 5).

Error of our formula for bulk fall speeds resides mostly within 5% and 20% for rain drops and ice particles (Fig. 4.6, Fig. 4.7), respectively, comparing to the theoretical values. The relative RMSE is about 1.4% for raindrops and 4% for ice particles. For both raindrops and ice particles, the relative error is usually higher for smaller particles. Low apparent particle density also gives higher error in our formula.

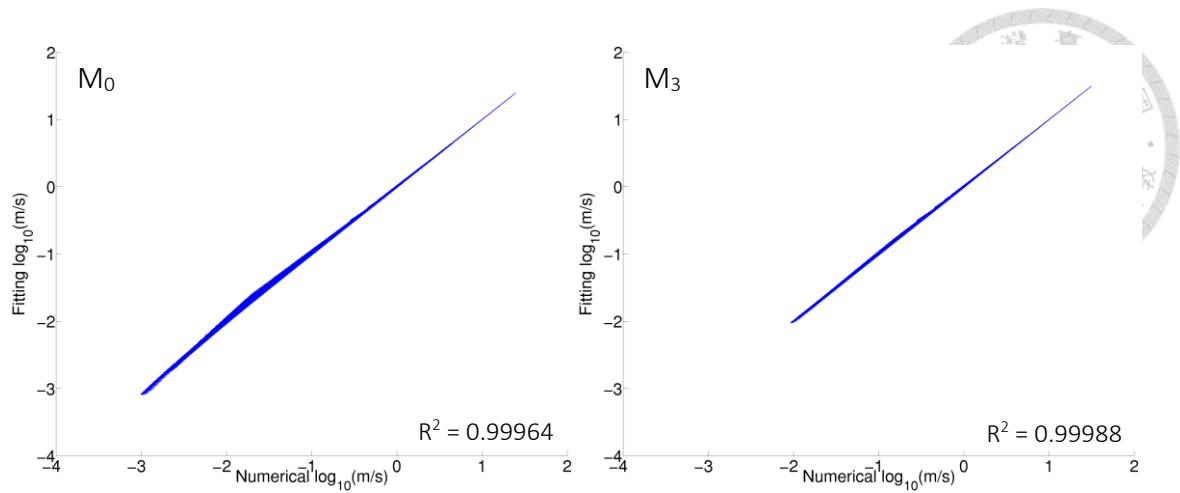


Fig. 4.6: Integral comparison between our parameterization formula for ice particles and the values derived from Böhm (1989). Gamma PSD parameters are in the range of $0 \leq \mu \leq 5$ and $0 \leq A \leq 60 \text{ mm}^{-1}$. The horizontal axis stands for the numerical integration using Böhm (1989); the vertical axis stands for the parameterization integrals in this study. Left: 0th moment kernel; right: 3rd moment kernel.

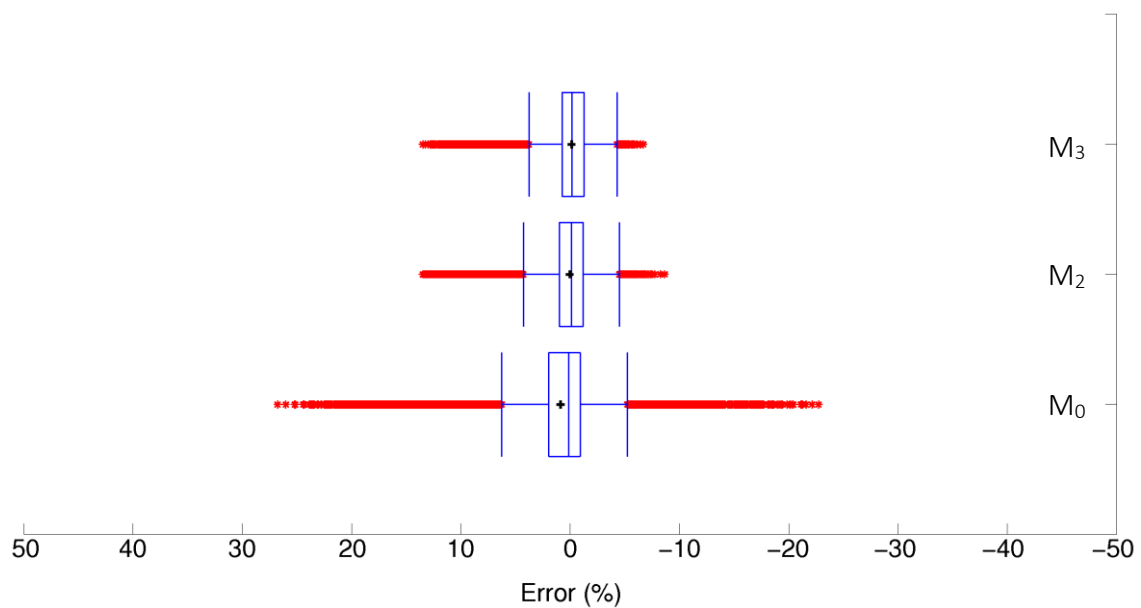


Fig. 4.7: Integral error of our formula for ice particles' comparing to numerical integral derived from Böhm (1989). From top to bottom are the 3rd, 2nd, and 0th moment kernel respectively.

4.3 One-dimension simple dynamics test

A simple dynamical comparison similar to Milbrandt and McTaggart-Cowan (2010) was conducted for raindrop fall speed parameterization to evaluate the accumulated difference between bin model, 3-moment bulk parameterization with our formula and

existing formulas. The only physical process considered is gravitational sedimentation and all other processes except ground removal are omitted for simplification.

$$\left\{ \begin{array}{l} \text{Bin: } \frac{\partial N}{\partial t} + \frac{\partial(v_t N)}{\partial z} = 0, \quad N = N(D, z, t) \\ \text{Bulk: } \frac{\partial M_{\langle k \rangle}}{\partial t} + \frac{\partial(M_{\langle k \rangle} V_{t \langle k \rangle})}{\partial z} = 0, \quad M_{\langle k \rangle} = M_{\langle k \rangle}(z, t) \end{array} \right. \quad (4.5)$$

The space-temporal finite difference scheme is 1st order upstream scheme as the following:

$$\left\{ \begin{array}{l} \text{Bin: } N_{D,j}^{\tau+1} = N_{D,j}^{\tau} - \frac{\Delta t}{\Delta z} (v(D, z_{j+1}) \cdot N_{D,j+1}^{\tau} - v(D, z_j) \cdot N_{D,j}^{\tau}) \\ \text{Bulk: } M_{\langle k \rangle, j}^{\tau+1} = M_{\langle k \rangle, j}^{\tau} - \frac{\Delta t}{\Delta z} (M_{\langle k \rangle, j+1}^{\tau} v_{\langle k \rangle, j+1}^{\tau} - M_{\langle k \rangle, j}^{\tau} v_{\langle k \rangle, j}^{\tau}) \end{array} \right. \quad (4.6)$$

with $\Delta t = 1/64$ s and $\Delta z = 1$ m, giving a Courant number ~ 0.25 for fall speed at 16 m/s. A bell shape vertical distribution with $N_0 = \cos^2[\pi(Z - Z_0)/2\sigma]$ is given at $Z_0 = 1850$ m with constant $\sigma = 150$ m; for the rest of the PSD parameters, they are set as $\mu = 3$, and $\Lambda = 3 \text{ mm}^{-1}$. The model uses three-moment scheme with the 0th, 2nd and 3rd moment. The air property is prescribed as standard atmosphere from 0 to 2000 meters above ground. Each moment is evaluated from sedimentation derived time derivative at each time step and height level, and then transformed back to parameters used in gamma distribution function for the use in the next step. The conversion method follows Tsai and Chen (2020) as the following:

$$\left\{ \begin{array}{l} \mu = -\frac{3(2\zeta - 1) + \sqrt{8\zeta + 1}}{2(\zeta - 1)}, \quad \zeta \equiv \frac{M_{\langle 2 \rangle}^3}{M_{\langle 0 \rangle} M_{\langle 3 \rangle}^2} \\ \Lambda = \frac{M_{\langle 2 \rangle}}{M_{\langle 3 \rangle}} \cdot (\mu + 3) \\ N_0 = M_{\langle 0 \rangle} \cdot \frac{\Lambda^{\mu+1}}{\Gamma(\mu + 1)} \end{array} \right. \quad (4.7)$$

The test results are shown in Fig. 4.8. As expected, the bulk parameterizations may behave quite differently from the bin model, as bin model retains more information while bulk parameterization only preserves the conservation of 3 given moments. The test

shows that the power-law implementation like WDM-6 gives drastically different results comparing to the one with numerically integrated theoretical terminal velocity. Results produced by the formulas used in the Thompson scheme behave surprisingly well, perhaps because the prescribed DSD does not cover the range of very large droplets where the Thompson scheme tends to underestimate the fall speed.

We also noticed that the limit of μ , as in Tsai and Chen (2020), is required in all bulk PSD parameterizations even for the one with numerically integrated theoretical values. As all other dynamical processes are omitted, gravitational sorting becomes significant and thus the bulk parameterization may result in extremely large μ and λ after a certain integration steps. While those extreme values usually come with very small N_0 and thus do not contribute much to the total kernel integral, such phenomenon may cause numerical instability and floating point overflow and hence should be carefully dealt with.

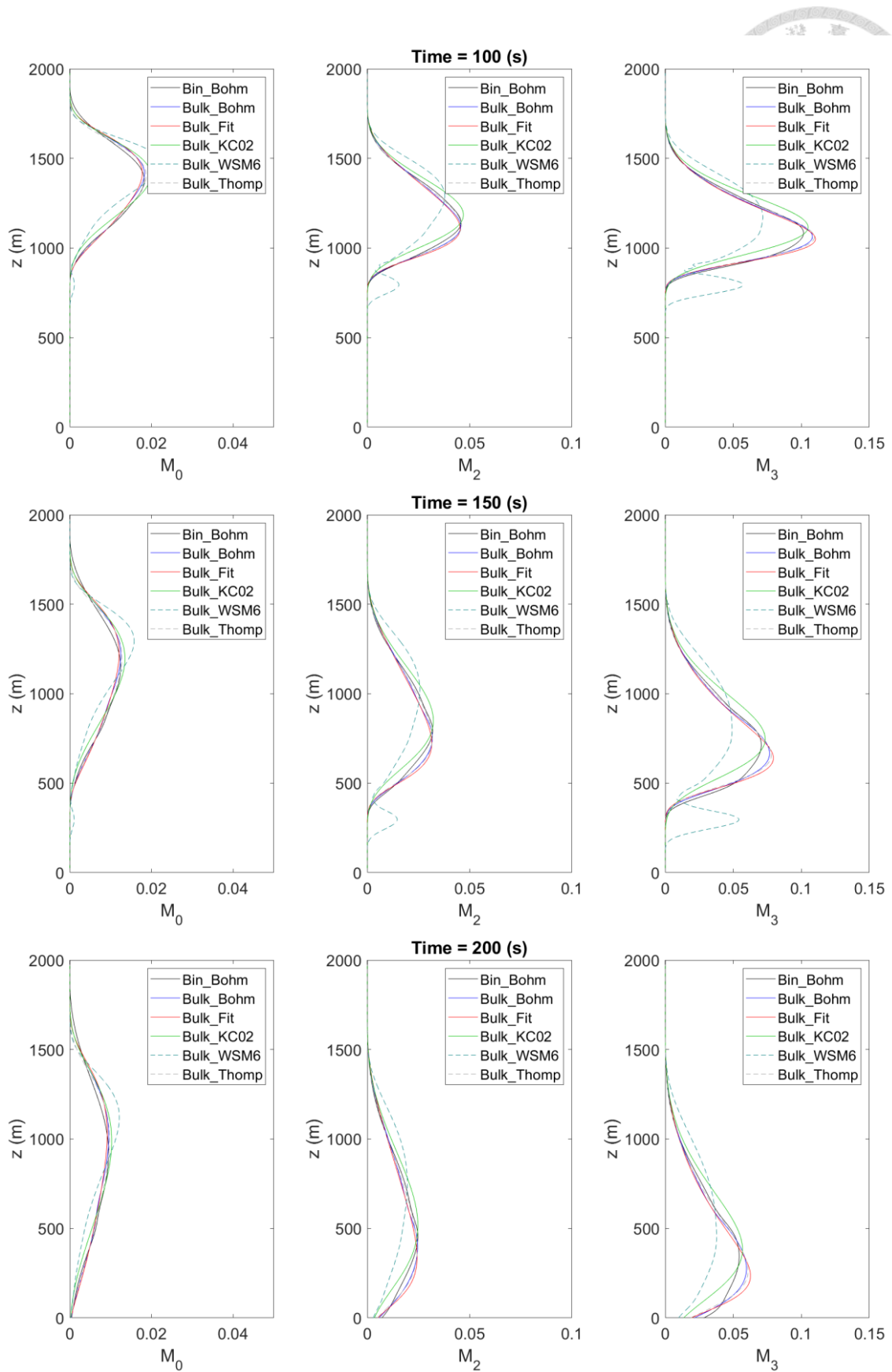


Fig. 4.8: 1-D simple dynamics test results. From top to bottom: the result at 100 (s), 150 (s), 200 (s) in model time. From left to right: the 0th, 2nd, and 3rd moment-height profile.

Chapter 5 Discussion



Large errors of our parameterization formulas mainly occur in two situations – sharp change of exponent in power-law relation with diameter and the effect of viscosity for small particles. The viscous limit suggests that terminal velocity is in proximity to D^2 . However, the flow regime quickly shifts to Oseen flow as the particle gets larger, which results in terminal velocity in proximity to D . The scaling then shifts to $D^{1/2}$ or less as derived from the boundary layer theory in the range of millimeters in diameter. Such a change may hardly be described by simple formulation lying within the integration constrain for bulk parameterization, resulting in higher error. The error from the effect of viscosity is mainly caused by our simplification of using air density instead of pressure and temperature separately. As stated in the Oseen flow theory, the creeping motion, that dominates the flow dynamics for lower Reynold's number, is highly related to the viscosity of air, which depends mostly on temperature. Our formula does not account for such an effect, hence resulting in higher error for small particles. As for computation efficiency, our formulas usually require two to three times as much as those of single-term formulas, primarily because our formulas consist of two to three terms and the efficiency bottleneck is mostly from the evaluation of the gamma function.

5.1 Raindrops

Best (1950), Atlas et al. (1973), and Lhermitte (1990) already proposed several formulas in form of exponential asymptotic function, which is intuitive based on experiments performed by Gunn and Kinzer (1949). Nevertheless, data from Gunn and Kinzer (1949) barely covers the viscous flow regime at the smaller diameter end of his

experiment, thus most previous equations do not include the viscous flow scaling which is proportional to D^2 ; instead, they behave as normal exponential function and scale to D . Our formula attempts to deal with this property by modifying an exponential asymptotic function with an extra power-law multiplier, thus consists three terms instead of two terms comparing to the most-comprehensive formulas proposed in previous studies. The resulting $d \ln(v) / d \ln(D)$ matches the values derived directly from Böhm (1992) between 0.5 mm to 8 mm in diameter (Fig. 5.1). Although such mathematical behavior may be achieved by adding another exponent term similar to the approach by Best (1950) that gives acceptable accuracy, the products of these formulas with gamma distribution function cannot be analytically integrated, and thus being unacceptable for our goal.

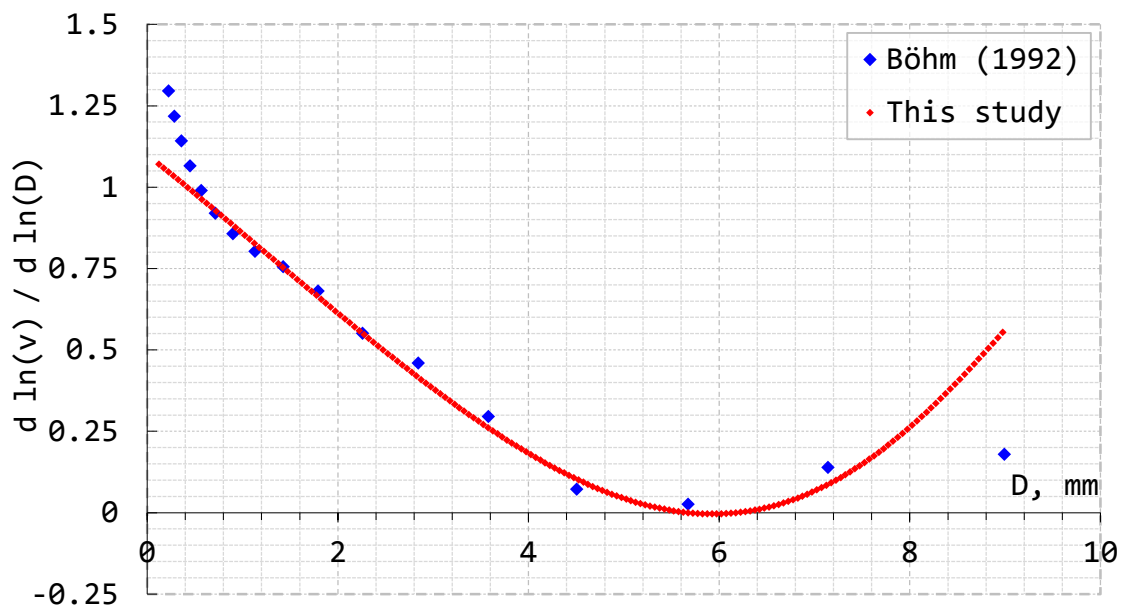


Fig. 5.1: The exponent of power-law relation between terminal velocity and diameter for raindrops.

Moreover, according to the theoretical calculation from Böhm (1992), air density may not follow a simple constant power-law relation for all droplets' diameter (Fig. 5.2). Such behavior is, however, not shown in previous experimental studies as those measurements (e.g. Gunn and Kinzer, 1949; Yu et al., 2016) are limited to single pressure and temperature conditions. The relation between terminal velocity and air density is

often treated as a simple power-law with exponent lying between -0.4 and -0.5 in most parameterization formula in previous studies. This may be linked with the terminal velocity derivation under Oseen flow regime for large particle asymptote (equation 2.7). This problem has been dealt with in our approach by adding putting air density dependence in the fitting coefficients in equation (4.1). In previous studies, the constant exponent in the air density term may introduce significant error in the formula.

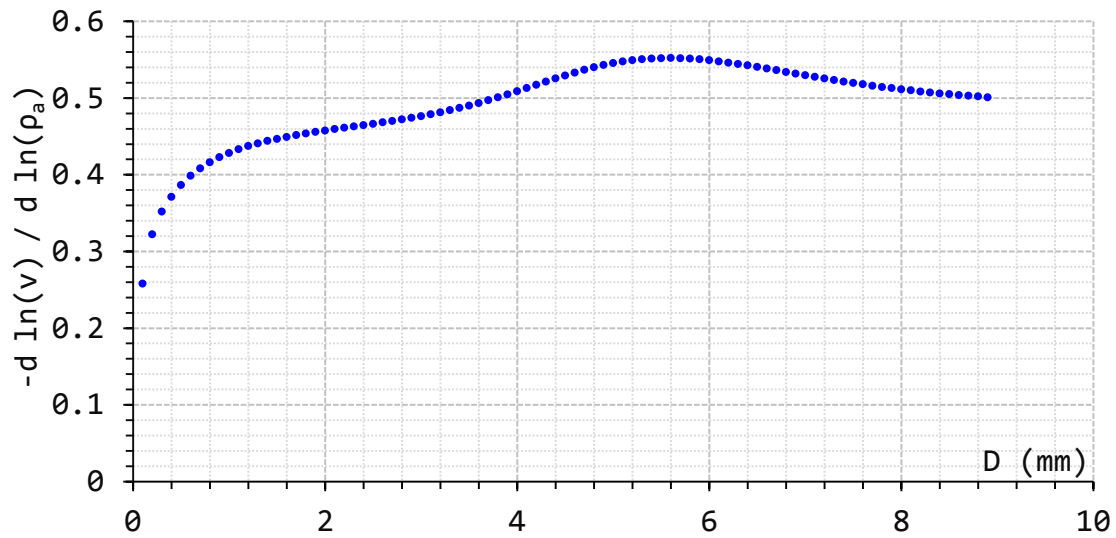
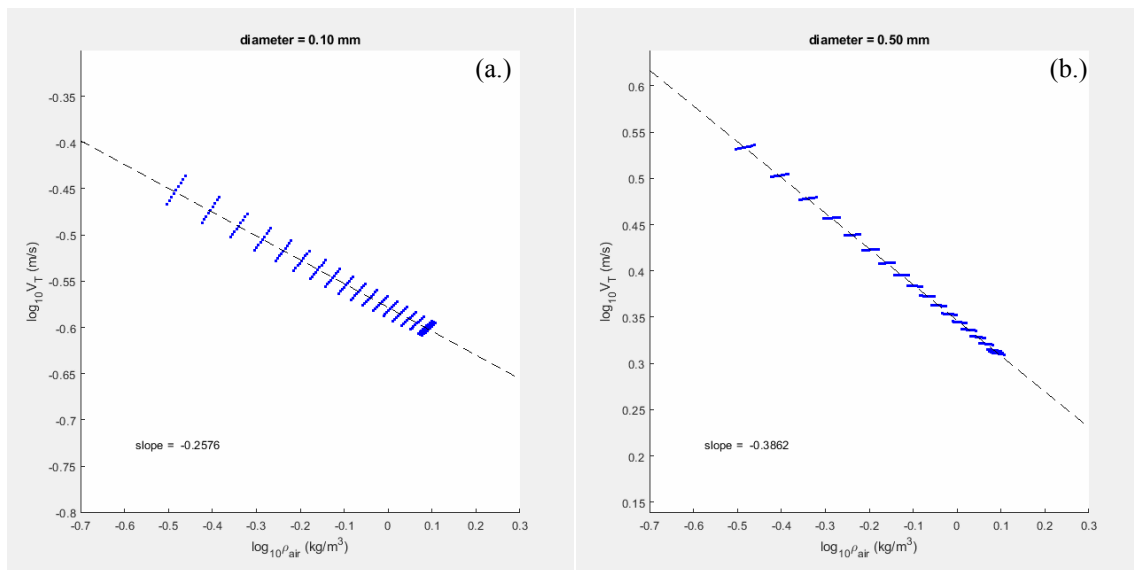


Fig. 5.2: Exponent in power-law relation between terminal velocity of raindrops and air density as a function of diameter under standard atmosphere profile.



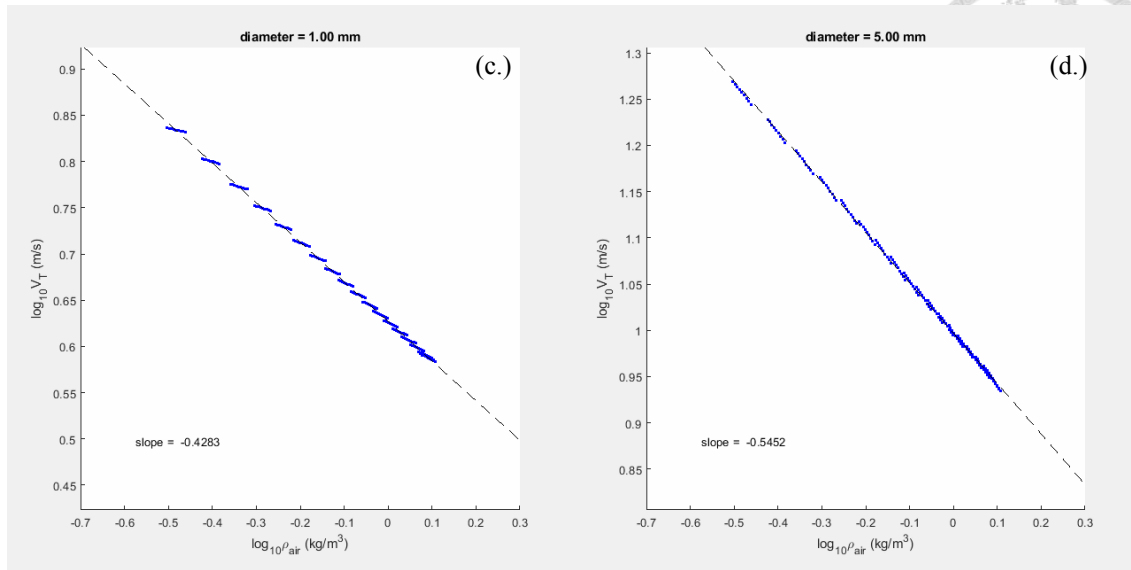


Fig. 5.3: Regression between terminal velocity and air density in Böhm (1992) at (a.) $D = 0.1$ mm, (b.) $D = 0.5$ mm, (c.) $D = 1$ mm, and (d.) $D = 5$ mm.

Khvorostyanov and Curry (2002) approached the problem with a different perspective by analyzing the relationship between the Best number and particle diameter, which can be used as a method to diagnose the optimal power-law relation of fall speed according to a given set of PSD parameters. This approach also retains its usability in bulk parameterization as a set of power-law parameters that can be derived directly from input variables and then output accordingly as an analytically integrated value. However, their study adopted a different shape deformation correction, resulting in an underestimation in the terminal velocity for median-sized droplets around 1 mm in diameter, and overestimation for larger droplets. The parameterization also does not specify the selection of optimal size to evaluate the power-law coefficients given a gamma distribution function. Since the derived exponent term of fall speed changes drastically with diameter, the evaluation of optimal diameter determining the power term may have significant impact on accuracy, especially for the situation where size distribution function is wider and covering a large range of diameters.

While Böhm (1992) suggested that linear correction is accurate to a certain extent, higher order correction in the form of polynomial is available (e.g. Brandes, 2002). However, all those corrections only consider the correspondent of droplets' diameter, while air density may theoretically have significant effect. Nonetheless, the lack of experimental data for deformation correction involving air density renders it implausible to apply such effect in our data derivation. Experiments conducted by Yu et al. (2016) gave a brief glimpse of decently accurate terminal velocity measurements under atmospheric conditions with slightly lower pressure level (~960 hPa) than at sea level as for Gunn and Kinzer (1949). Although both the predictions by Böhm (1992) and our parameterization formula show close proximity towards the experiment results and 9th-order polynomial expansion from Foote and duToit (1969) (Fig. 5.4), further inspections may be required to examine the behaviors of droplet shapes under lower atmospheric pressure level, since the pressure difference between the environment in Yu et al. (2016) and at sea level is comparably small to the extent of whole troposphere.

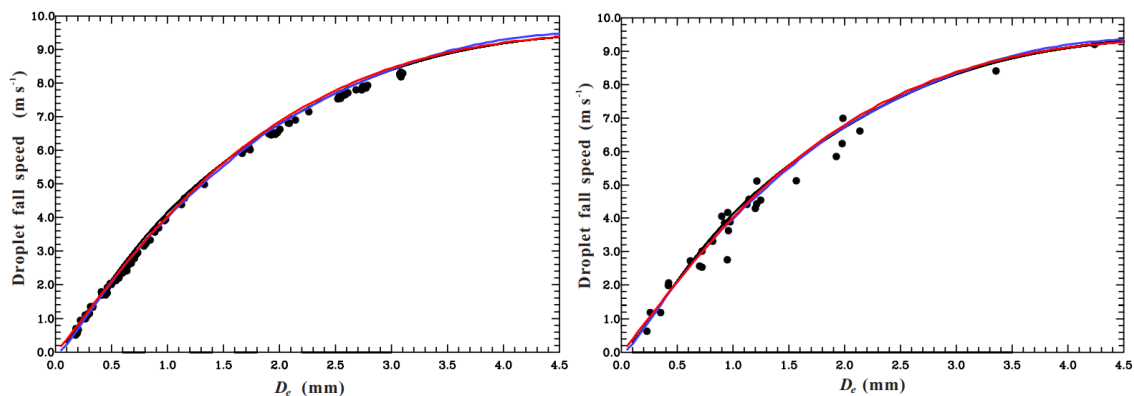
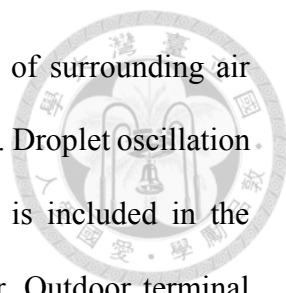


Fig. 5.4: Comparison between Böhm (1992, blue solid lines), our formula (red solid lines), 9th-order polynomial expansion from Foote and duToit (1969, black solid lines), and experimental results from Yu et al. (2016, black dots) in indoor measurements (left) and outdoor measurements (right). Indoor measurements are conducted under 956.4 hPa and 30.3 °C, while outdoor measurements are conducted under 960.6 hPa and 25.5 °C.

The scattering in the outdoor in-situ terminal velocity observations is likely



associated with factors including droplet oscillation and turbulence of surrounding air (Pruppacher and Klett, 2010; Testik and Barros, 2007; Yu et al., 2016). Droplet oscillation is widely believed to spread out the droplets' aspect ratio, which is included in the theoretical calculation of droplets' terminal velocity as a parameter. Outdoor terminal velocity measurements from Yu et al. (2016, Fig. 5.4) suggest such effects are not negligible and should be considered when comparing theoretical predictions and values derived from observational data, especially for radar observations, which may also be sensitive to the shape of droplets.

5.2 Ice particles

For ice particles, multiple factors of complexity are introduced including particles' apparent density, shape and surface irregularity. Raindrops' shape, under the steady state assumption, may be considered as solely dependent on air property and droplet diameter. Coupled with constant density as the bulk density of water, the terminal velocity may be seen as a two-variable function. Ice particles are regarded as solids and can contain notches and hollows or trapped air packets inside them; therefore, shape, apparent density and surface irregularity have to be taken into consideration as independent parameters. The complexity gives the number of fitting coefficients much greater than the formula for raindrops. As the TableCurve 3D software may only fit functions with two parameters in one session, extra error is introduced in the process of fitting the first-step coefficients against apparent density in the second session. Particles with lower apparent density results in higher error as the relationship between each first-step coefficient and particle density becomes more non-linear as the apparent density approaches zero.

Unfortunately, the extra parameters also render it difficult to compare between our formula and experimental or observational data, which generally do not contain such details. As the shape of particles deviates from spherical, additional surface area slows the particles down, mathematically resulting in additional degrees of freedom. therefore we may give a range of optimal aspect ratio values for each type of particles in a given set of data.

Mitchell and Heymsfield (2005) (MH05) suggested a framework using particles' maximum dimension along with parameterized area/mass-dimension relationship in power-law form to evaluate the terminal velocity. Following Khvorostyanov and Curry (2002), the framework may be used to diagnose with a set of optimal power-law relationship parameters between terminal velocity and particles' maximum dimension by incorporating the area/mass-dimension relationship:

$$\begin{cases} m = \alpha D_M^\beta \\ A = \gamma D_M^\sigma \end{cases} \quad (5.1)$$

where D_M is the maximum dimension of the particle. The Best number in use is, however, different from that defined by Böhm (1989) with the following form:

$$X \equiv \frac{2mg\rho_a D_M^2}{A\eta^2}. \quad (5.2)$$

MH05 also provided a less complicated parameterization of turbulence correction for graupel and hail as a power-law of X with stated constant coefficients. However, while their study did incorporate the apparent density and cross-section area ratio of particles in the formula, the effect of particles' shape deviating from being spherical is not thoroughly evaluated in their formulation. Their terminal velocity is instead computed as:

$$v \equiv \frac{N_{Re}\eta}{\rho_a D_M} = \begin{cases} \frac{N_{Re}\eta}{\rho_a D} \cdot \phi^{1/3}, & \text{for oblates;} \\ \frac{N_{Re}\eta}{\rho_a D} \cdot \phi^{-2/3}, & \text{for prolates.} \end{cases} \quad (5.3)$$



For oblate particles, the calculations are identical to those of Böhm (1989) and MH05. However, the formulas evaluating terminal velocity of prolate spheroids are different. For small particles with $X \ll 1$, with the approximation of $\sqrt{1+\epsilon} \approx 1 + \epsilon/2$, it can be shown that the terminal velocity predicted in MH05 is higher than the one in Böhm (1989) by a factor of $\phi^{2/3}$. For large particles with very large X , the deviation between two framework reduce to the second order, thus the relative difference vanishes, with MH05 gives only slightly larger values. (Fig. 5.5)

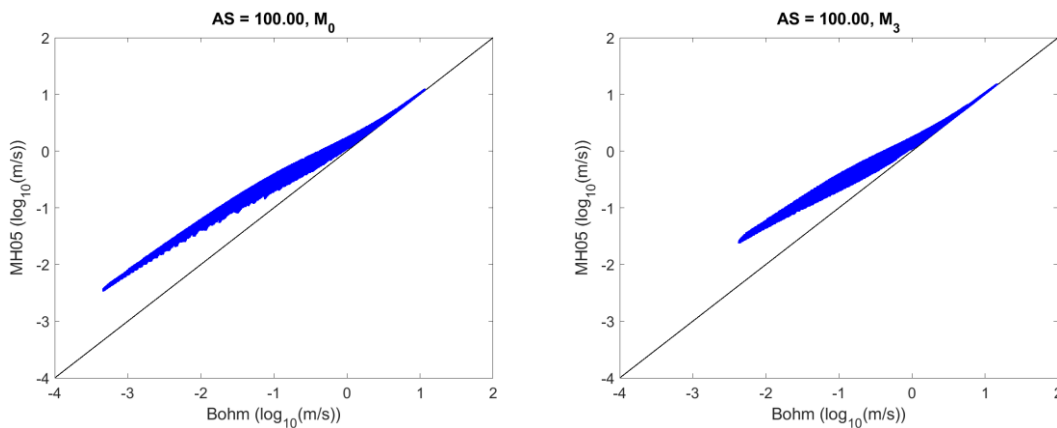
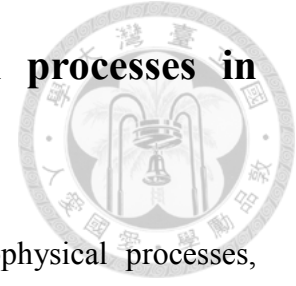


Fig. 5.5: The difference between Böhm (1989) and MH05 for prolates with aspect ratio of 100.

Most studies focusing on theoretical terminal velocity predictions only regard the orientation of ice particles as having maximum downward projected area. However, observational and simulation studies suggest falling crystals may experience rotation and pitch-glide oscillation (Pruppacher and Klett, 2010), which may similarly have impacts on matching observational-derived data with theoretical values. If the probability of the pitch angle is known, our parameterization may still be applied by imposing a probability density function (PDF) of projected ϕ if the PDF can be expressed as a gamma function.

5.3 Incorporation with other microphysical processes in models



Fall speed of hydrometers is also relevant in other microphysical processes, including ventilation effect in condensation/evaporation, and collision coalescence. To evaluate ventilation effect, the ventilation coefficient, f_v , is commonly used:

$$\frac{dm}{dt} = 4\pi r f_g f_v (\rho_{v,\infty} - \rho_{v,drop}) \quad (5.4)$$

Where r is the radius of droplet, τ is the mass diffusivity, f_g is the kinetic correction factor, $\rho_{v,\infty}$ is the environmental vapor density, and $\rho_{v,drop}$ is the vapor density at the surface of droplet. Hence the bulk condensation growth may be written as:

$$\int_0^{\infty} \frac{dr^k}{dt} N(r) dr = \int_0^{\infty} \frac{k\tau f_g f_v (\rho_{v,\infty} - \rho_{v,drop})}{\rho_w} r^{k-2} N(r) dr, \quad (5.5)$$


with the ventilation coefficient equation:

$$f_v = \sqrt[3]{N_{Sc}} \sqrt{N_{Re}}, \quad (5.6)$$

where N_{Sc} is the Schmidt number (Ji and Wang, 1999). The ventilation coefficient in models are usually fitted against the Best number, X , as polynomial expansions (Ji and Wang, 1999):

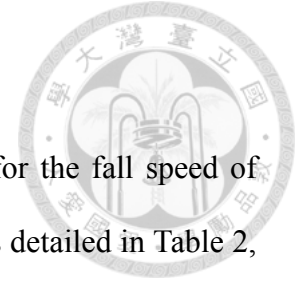
$$f_v \approx \sum_n a_n X^n. \quad (5.7)$$

Unfortunately, such expansion will not emit analytical integral for equation (5.5) along with our terminal velocity formulas, given the complicated relation between the Best number and terminal velocity. Incorporation between our formulas and ventilation coefficient requires either fitting of f_v against particles' diameter as gamma-distribution-typed functions or expand the coefficient against terminal velocity itself instead of Best number.



As for the evaluation of hydrometeor collision coalescence, similar treatments may also be plausible. However, given the mathematical complexity of collection efficiency, it may be quite difficult to achieve adequate accuracy with such approach. Applying SNAP-KT method (Chen et al., 2013) directly to the equation prior to integration could be another route towards more accurate bulk-parameterized collision coalescence growth. A likely more accurate approach is to perform numerical integration of the bulk microphysical formulas with detailed kernels and then do statistical fitting on the results with other methods suggested in Chen et al. (2013).

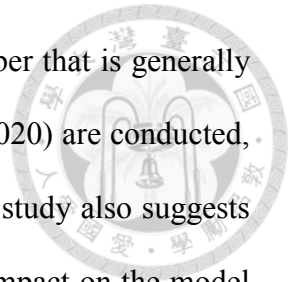
Chapter 6 Conclusion



This study proposes a new set of parameterization formulas for the fall speed of precipitation particles in the form of equation. (4.1) with parameters detailed in Table 2, which can be analytically integrated with 3-moment gamma-type PSD. The formulas may be implemented in numerical models with bulk microphysics parameterizations. The formula is derived by fitting theoretically calculated data proposed by Böhm (1992) for raindrops and mainly Böhm (1989) for ice particles. The terminal velocity formula for ice particles may be applied to all types of particles using the aspect ratio as the shape parameter under the spheroidal particle assumption. The deviations lie mostly within 5% for raindrops and 20% for ice particles, with integral relative RMSE of 1.4% and 4% respectively, comparing to the predictions by Böhm (1992) for raindrops and Böhm (1989) for ice particles. Errors are larger for small particles as air density is used as the parameter for air property instead of temperature and pressure. Terminal velocity for small particles is more susceptible to viscosity as described by Stokes flow. For raindrop terminal velocity parameterization, our formula gives much better approximation comparing to formulas deployed in WRF model, which gives the relative RMSE of 8.1% for WDM6 and 7.5% for Thompson scheme in integrals. Part of our error reduction is achieved by including non-conventional air density treatment which allows our formula to have varying exponent for air density in form of power-law relation.

A simple 1D sedimentation-only dynamic model test is conducted to examine the usability of the raindrop parameterization formula. Results show close proximity between our formula and numerically integrated values using Böhm (1992) under bulk parameterization scheme. However, special treatment for large μ is still required in order


to guarantee sufficient numerical stability, even under Courant number that is generally considered to be stable. Offline tests comparing to Tsai and Chen (2020) are conducted, with our formula giving results in the same scale (not shown). That study also suggests that terminal velocity, especially for ice particles', may have large impact on the model results. Online tests using WRF model with 3-moment bulk parameterization schemes should be conducted to evaluate the behavior and accuracy of our formula in a more complex model framework.

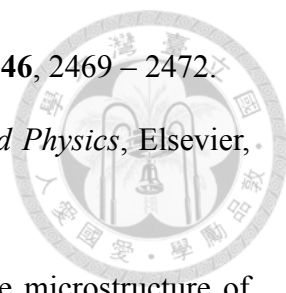


REFERENCE



- [1] Atlas, D., R. C. Srivastava, and R. S. Sekhon, 1973: “Doppler radar characteristics of precipitation at vertical incidence.” *Rev. Geophys.*, **11**, 1–35.
- [2] Atlas, D., and C. W. Ulbrich, 1977: “Path and Area-Integrated Rainfall Measurement by Microwave Attenuation in the 1–3 cm Band.” *J. Appl. Meteor.*, **16**, 1322–1331.
- [3] Best, A. C., 1950: “Empirical formulae for the terminal velocity of water drops falling through the atmosphere.” *Q. J. R. Meteorol. Soc.*, **76**, 302 – 311.
- [4] Böhm, H. P., 1989: “A General Equation for the Terminal Fall Speed of Solid Hydrometeors.” *J. Atmos. Sci.*, **46**, 2419–2427.
- [5] Böhm, H. P., 1991: “Review of flow characteristics and kinematics of hydrometeors in free fall.” *Atmos. Res.*, **26**, 285–302.
- [6] Böhm, H. P., 1992: “A general hydrodynamic theory for mixed-phase microphysics. Part I: Drag and fall speed of hydrometeors.” *Atmos. Res.*, **27**, 253–274.
- [7] Brandes, E. A., G. Zhang, and J. Vivekanandan, 2002: “Experiments in Rainfall Estimation with a Polarimetric Radar in a Subtropical Environment.” *J. Appl. Meteor.*, **41**, 674–685.
- [8] Chen, J. P., and D. Lamb, 1994: “The Theoretical Basis for the Parameterization of Ice Crystal Habits: Growth by Vapor Deposition.” *J. Atmos. Sci.*, **51**, 1206–1222.
- [9] Chen, J. P., I. C. Tsai, and Y. C. Lin, 2013: “A statistical–numerical aerosol parameterization scheme.” *Atmos. Chem. Phys.*, **13**, 10483–10504.
- [10] Chen, J. P., and T. C. Tsai, 2016: “Triple-Moment Modal Parameterization for the Adaptive Growth Habit of Pristine Ice Crystals.” *J. Atmos. Sci.*, **73**, 2105–2122.

- 
- [11] Foote, G. B., and P. S. duToit, 1969: “Terminal velocity of raindrops aloft.” *J. Appl. Meteorol.*, **8**, 249–253.
- [12] Gunn, R., and G. D. Kinzer, 1949: “The Terminal Velocity of Fall For Water Droplets in Stagnant Air.” *J. Meteor.*, **6**, 243–248.
- [13] Ji, W., and P. K. Wang, 1999: “Ventilation Coefficients for Falling Ice Crystals in the Atmosphere at Low–Intermediate Reynolds Numbers.” *J. Atmos. Sci.*, **56**, 829–836.
- [14] Khvorostyanov, V. I., and J. A. Curry, 2002: “Terminal velocities of droplets and crystals: Power laws with continuous parameters over the size spectrum.” *J. Atmos. Sci.*, **59**, 1872–1884.
- [15] Lhermitte, R., 1990: “Attenuation and Scattering of Millimeter Wavelength Radiation by Clouds and Precipitation.” *J. Atmos. Oceanic Technol.*, **7**, 464–479.
- [16] McFarquhar, G. M., T. Hsieh, M. Freer, J. Mascio, and B. F. Jewett, 2015: “The Characterization of Ice Hydrometeor Gamma Size Distributions as Volumes in N_0 – λ – μ Phase Space: Implications for Microphysical Process Modeling.” *J. Atmos. Sci.*, **72**, 892–909.
- [17] Marshall, J. S., and W. McK. Palmer, 1948: “Shorter Contribution: The Distribution of Raindrops with Size.” *J. Meteor.*, **5**, 154–166.
- [18] Milbrandt, J. A., and R. McTaggart-Cowan, 2010: “Sedimentation-Induced Errors in Bulk Microphysics Schemes.” *J. Atmos. Sci.*, **67**, 3931–3948.
- [19] Mitchell, D. L., and A. J. Heymsfield, 2005: “Refinements in the Treatment of Ice Particle Terminal Velocities, Highlighting Aggregates.” *J. Atmos. Sci.*, **62**, 1637–1644.
- [20] Pruppacher, H.R., and J.D. Klett, 2010: *Microphysics of Clouds and Precipitation*, Springer, 958 pp.

- 
- [21] Rogers, R. R., 1989: “Raindrop collision rates”, *J. Atmos. Sci.*, **46**, 2469 – 2472.
- [22] Rogers, R. R., and M. K. Yau, 1989: *A Short Course in Cloud Physics*, Elsevier, 304 pp.
- [23] Testik, F. Y., and A. P. Barros, 2007: “Toward elucidating the microstructure of warm rainfall: A survey.” *Rev. Geophys.*, **45**, Z57–Z77.
- [24] Tokay, A., and D. A. Short, 1996: “Evidence from Tropical Raindrop Spectra of the Origin of Rain from Stratiform versus Convective Clouds.” *J. Appl. Meteor.*, **35**, 355–371.
- [25] Tsai, T. C., and J. P. Chen, 2020: “Multimoment Ice Bulk Microphysics Scheme with Consideration for Particle Shape and Apparent Density. Part I: Methodology and Idealized Simulation.” *J. Atmos. Sci.*, **77**, 1821–1850.
- [26] Ulbrich, C. W., 1983: “Natural Variations in the Analytical Form of the Raindrop Size Distribution.” *J. Climate Appl. Meteor.*, **22**, 1764–1775.
- [27] Willis, P. T., F. Marks, and J. Gottschalck, 1999: “Rain Drop Size Distributions and Radar Rain Measurements in South Florida.” https://www.aoml.noaa.gov/hrd/FlBay/florida_bay_99.html.
- [28] Yu, C. K., P. R. Hsieh, S. E. Yuter, L. W. Cheng, C. L. Tsai, C. Y. Lin, and Y. Chen, 2016: “Measuring droplet fall speed with a high-speed camera: indoor accuracy and potential outdoor applications.” *Atmos. Meas. Tech.*, **9**, 1755–1766.